Interaction between soot particles and NO_x during dielectric barrier discharge plasma remediation of simulated diesel exhaust

Rajesh Dorai[a)]
University of Illinois, Department of Chemical Engineering, 1406 West Green Street, Urbana, Illinois 61801

Khaled Hassouni[b)]
LIMHP, UPR1311-CNRS, Université Paris Nord, Avenue J. B. Clément 93430, Villetaneuse, France

Mark J. Kushner[c)]
University of Illinois, Department of Electrical and Computer Engineering, 1406 West Green Street, Urbana, Illinois 61801

(Received 27 June 2000; accepted for publication 29 August 2000)

Plasma remediation is being investigated as a means to remove NO_x from combustion effluent and from diesel exhausts in particular. Soot particles are inevitably present in actual exhausts and may, through heterogeneous chemistry, affect the remediation process. In this article, a computational investigation of the effect of soot on the plasma chemistry of NO_x removal in a simulated diesel exhaust processed in a dielectric barrier discharge reactor is presented using a zero-dimensional global-kinetics simulation. A surface chemistry model is employed to describe soot oxidation by O and OH radicals, and soot-NO_x interactions. The NO_x chemistry may be substantially affected by the reactions at the soot surface. In particular, for soot particles having densities of 10^8 cm^{-3} and diameters of 100 nm, significant increases of NO are obtained when taking into account $NO_2 \rightarrow NO$ conversion on the soot surface. Heterogeneous reaction of NO_2 also results in an increase in the gas-phase OH density which results in the increased formation of HNO_2, thereby adding to the NO_x remediation. $NO_2 \rightarrow NO$ heterogeneous conversion also results in an increase of CO and a subsequent reduction of the soot mass. The mechanism for soot-NO_x interactions depends on the deactivation of active hydrocarbon radicals on the soot. © *2000 American Institute of Physics.* [S0021-8979(00)03023-1]

I. INTRODUCTION

The use of atmospheric nonthermal plasma processing in tandem with selective catalytic reduction has shown promise for the removal of nitrogen oxides (NO_x) in diesel combustion exhausts.[1–4] Nonthermal plasmas efficiently convert NO, the major NO_x compound in the exhaust, to NO_2.[5,6] The NO_2 can then be remediated to N_2 through selective catalytic reduction[7–9] in a process usually called plasma enhanced selective catalytic reduction (PE-SCR). A key advantage of PE-SCR is the selectivity of the oxidation process with respect to SO_x compounds, also usually present in diesel exhausts. Despite the oxidizing character of the plasma, the SO_2 molecule remains stable and undesirable SO_3 species are not formed, which could poison the NO_2 reduction catalysts.

Several experimental and numerical investigations have been performed on the discharge dynamics[10,11] and the chemical kinetics[12–14] in dielectric barrier discharge (DBD) reactors used for diesel exhaust treatment. Since the actual exhaust composition depends on the origin of the fuel, fuel-to-air ratio and compression ratio, these investigations are usually performed on model gases. Typical base case mixtures are, for example, $N_2/O_2/CO_2/H_2O = 75/10/10/5$ with NO, CO, or SO_2 at concentrations of 100–700 ppm, similar to those found in actual diesel exhausts. More recently, light hydrocarbons such as ethene (C_2H_4),[15] propene (C_3H_6)[1] and a propene/propane mixture (C_3H_6/C_3H_8)[16] were also included in the exhaust at concentrations of 100–1000 ppm to investigate the consequences of unburned hydrocarbons (UHCs) on NO_x removal. Both experiments and modeling showed that NO_x remediation in DBDs at energy depositions of 50–60 J/L may increase up to 20% when propene is present at concentrations of 100s ppm.[16] An increase in the $NO \rightarrow NO_2$ oxidation through reactions of NO with hydrocarbon oxides formed in the plasma is largely responsible for this improvement. Reaction of NO_2 with the hydrocarbon-initiated reaction intermediates results in the formation of organic nitrates and nitrites, which add to the NO_x remediation. Further NO_x remediation is also obtained through the formation of nitric and nitrous acids.

Another step towards more realistic modeling of plasma treatment of exhaust is accounting for carbonaceous particles in the exhaust. Soot particles in typical diesel exhausts have mass concentrations of 20–200 mg/m^3.[17] The average geometric diameter and particle density of the soot particles depend on the combustion regime. Typical values are around 100 nm[18] and 10^8 cm^{-3},[17,19] which are high enough to initiate heterogeneous chemistry. Soot influences the chemistry of NO_x plasma remediation dominantly through NO_2-soot interactions[20,21] and influences the ionization kinetics

[a)]Electronic mail: dorai@uiuc.edu
[b)]Electronic mail: hassouni@limhp.univ-paris13.fr
[c)]Author to whom correspondence should be addressed; electronic mail: mjk@uiuc.edu

through electron and ion attachment to the particles. The resulting changes of electron density and temperature may then affect the rates of electron-impact processes.

In this article, the consequences of soot particles on the plasma chemistry in simulated diesel exhaust gas processed in a DBD reactor are numerically investigated. The zero-dimensional global kinetics simulation GLOBAL_KIN was modified to address heterogeneous chemistry using a quasi-homogeneous gas-phase assumption.[16] NO_x-soot interactions, heterogeneous reactions of radicals such as O and OH and the effect of soot on the ionization kinetics were addressed. We found that in the presence of soot, NO_x remediation improved by nearly 10%. It was also found that, in the presence of soot, higher energies were required for the remediation of a given amount of NO. GLOBAL_KIN is described in Sec. II. The results from our parametric studies on the NO_x chemistry are in Sec. III. Section IV contains our concluding remarks.

II. DESCRIPTION OF THE MODEL

The DBD reactor for our study is sustained between dielectric slabs backed by planar electrodes. The discharge is pulsed creating a filamentary plasma with current durations of $\approx 10^{-7}$ s. The discharge consists of arrays of few tens of microstreamers per cm^2 having radii of tens to hundreds of microns.[10] The model used in this work describes the reactor in terms of volume averaged quantities. Although spatial variations are ignored, this approach enables the use of a detailed chemical model. The reaction set includes electron-impact processes that occur during the discharge pulse which result in ionization, dissociation and attachment processes: heavy species reactions that describe neutral chemistry and charge exchange, ion-conversion and ion recombination processes. The chemical model involves 170 species and 752 reactions and is discussed in detail in Ref. 22. To investigate exhausts containing soot particles, a heterogeneous chemistry model was developed and incorporated into GLOBAL_KIN.

The source terms for the gas phase reactions are obtained from the species concentration and reaction rate coefficients using

$$W_{i-g}=\sum_j \left\{ (a_{ij}^{(2)}-a_{ij}^{(1)})k_j \prod_l n_l^{a_{ij}^{(1)}} \right\}, \tag{1}$$

where $a_{ij}^{(1)}$ and $a_{ij}^{(2)}$ denote the left hand side and right hand side stoichiometric coefficients of species i in reaction j. The term k_j is the rate constant of reaction j which depends on the gas temperature and is calculated using Arrhenius expressions for reactions involving only heavy species. The rate constants of electron-impact reactions are obtained as a function of electron temperature. These coefficients are obtained by solving the two-term spherical harmonic expansion of Boltzmann's equation for the electron energy distribution which is parametrized for several values of the reduced electric field.

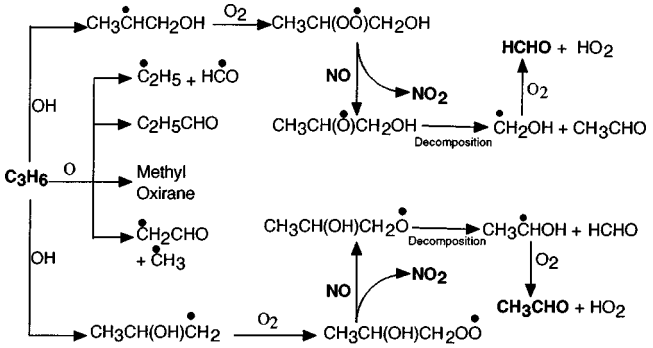

FIG. 1. Reaction mechanism for NO_x in the presence of UHCs.

A. Gas phase chemistry

The base gas mixture contained $N_2/O_2/H_2O/CO_2 = 79/8/6/7$ with 400 ppm of CO, 260 ppm of NO, 133 ppm of H_2, 500 ppm of propene and 175 ppm of propane. The last two gases are used as model UHCs. The details of the reaction mechanism used in the absence of soot are discussed in Refs. 14 and 16, and so we will only briefly describe the main governing reactions.

The reaction mechanism for NO_x chemistry is shown in Fig. 1. The NO_x chemistry is mainly driven by oxidation processes that result in the conversion of NO to NO_2. The radicals initiating the chemistry, O, N, and OH are produced by electron-impact processes

$$e+O_2 \rightarrow O+O+e, \tag{2}$$

$$e+N_2 \rightarrow N+N+e, \tag{3}$$

$$e+H_2O \rightarrow OH+H+e. \tag{4}$$

NO reduction occurs through the reaction with N atoms

$$N+NO \rightarrow N_2+O. \tag{5}$$

Reactions with O atoms and OH radicals result in NO oxidation

$$NO+O+M \rightarrow NO_2+M, \tag{6}$$

$$NO_2+OH+M \rightarrow HNO_3+M. \tag{7}$$

In the presence of UHCs, the key oxidant species are the OH and HO_2 radicals and the β-hydroxyalkyl peroxy radicals (βHAPs) $CH_3CH(OO)CH_2OH$ and $CH_3CH(OH)CH_2OO$. HO_2 is an intermediate produced by reactions of βHAPs. The βHAP radicals are produced through a two-step oxidation of propene initiated by OH, which is initially produced by electron impact of H_2O [Eq. (4)]. The β-hydroxyalkyl radicals CH_3CHCH_2OH and $CH_3CH(OH)CH_2$ are intermediate-species

$$C_3H_6+OH \rightarrow CH_3CHCH_2OH, \tag{8}$$

$$C_3H_6+OH \rightarrow CH_3CH(OH)CH_2, \tag{9}$$

$$CH_3CHCH_2OH+O_2 \rightarrow CH_3CH(OO)CH_2OH, \tag{10}$$

$$CH_3CH(OH)CH_2+O_2 \rightarrow CH_3CH(OH)CH_2OO. \tag{11}$$

The oxidation of NO then takes place following two pathways. The first one is a simple oxidation involving HO_2

$$HO_2+NO\rightarrow NO_2+OH. \quad (12)$$

The second channel involves the βHAP radicals

$$CH_3CH(OO)CH_2OH+NO\rightarrow CH_3CH(O)CH_2OH+NO_2, \quad (13)$$

$$CH_3CH(OH)CH_2OO+NO\rightarrow CH_3CH(OH)CH_2O+NO_2. \quad (14)$$

The radicals produced through the reactions of βHAPs with NO undergo thermal decomposition which ultimately leads to the formation of HO_2, formaldehyde (HCHO), and acetaldehyde (CH_3CHO)

$$CH_3CH(O)CH_2OH\rightarrow CH_2OH+CH_3CHO, \quad (15)$$

$$CH_2OH+O_2\rightarrow HCHO+HO_2, \quad (16)$$

$$CH_3CH(OH)CH_2O\rightarrow CH_3CHOH+HCHO, \quad (17)$$

$$CH_3CHOH+O_2\rightarrow CH_3CHO+HO_2. \quad (18)$$

These reactions lead to $NO\rightarrow NO_2$ conversion. The actual NO_x remediation from the exhaust is mainly due to the oxidation of NO_2 to HNO_3 [Eq. (7)] and

$$NO+OH+M\rightarrow HNO_2+M. \quad (19)$$

The fraction of NO_x that is actually converted to HNO_2 and HNO_3 ranges between 10% and 20%.[16]

B. NO_x soot interaction and soot oxidation models

The gas temperatures of interest are $\approx$453 K and the gas residence time is usually a few tenths of a second. Under these conditions soot growth and soot nucleation are kinetically limited and may be neglected. Similarly, the soot oxidation by molecular oxygen usually observed in combustion does not take place in DBDs since gas temperatures above 700 K are typically required for such processes to be important.[23] However, soot particles may undergo oxidation when reacting with plasma generated radicals such as O and OH which are effective oxidants for carbonaceous particles even at low temperature ($T\approx$300 K).[24,25] The oxidation of soot by OH is one of the major soot consumption processes in flames, and occurs with a reaction probability of $\approx$0.1, producing CO and H_2.[24] The oxidation of solid carbon by O atoms at low temperatures producing CO has been investigated only for solid graphite films. Reaction probabilities as high as 0.12 have been reported at 300 K.[25]

The interaction between NO_x and soot takes place through adsorption and reduction processes involving NO_2. The interaction of NO_x with carbonaceous particles was first considered in the context of atmospheric chemistry.[20,21,26–28] These studies indicated that reactions of soot with NO_2 lead to the formation of NO[26,27] and HNO_2.[28] At low temperatures ($T<$333 K) NO_2 once adsorbed tends to remain on the soot. The adsorption of NO_2 on *n*-hexane soot particles was investigated by Smity *et al.* who showed that, at 300 K, two adsorbates are formed, C–ONO and C–NO_2.[20,21,29] For temperatures higher than 350 K, a redox reaction of NO_2 occurs resulting in the desorption of NO and CO to the gas phase.

In principle, soot particles can also react with other radicals in the NO_x chemistry. However, the homogeneous gas-phase chemistry of these radicals, with the exception of the βHAPs, produces less frequencies several orders of magnitudes greater than their collision frequencies with soot particles. For example, the loss frequency of β hydroxyalkyl radicals by reaction with O_2 is approximately 10^8 s^{-1} compared to the collision frequency with soot particles of $\approx 10^4$ s^{-1} for a particle density of 5×10^8 cm^{-3} and a particle diameter of 150 nm. Consequently, the concentration of these radicals is mainly governed by the gas-phase chemistry and their interaction with soot may be neglected.

An exception is the βHAP radical which is consumed by NO with a frequency of $\approx 10^3$ s^{-1} for a NO density of 10^{16} cm^{-3}. Since there is little data on the reaction of βHAP radicals on soot particles, parametric studies on these rate coefficients were performed.

To take into account these heterogeneous processes, we developed the following surface reaction mechanism for soot particles (denoted by C_xH_y):

$$C_xH_y)+NO_2\rightarrow (C_{x-1}H_y)-C-NO_2, \quad (20)$$

$$(C_xH_y)+NO_2\rightarrow (C_{x-1}H_y)-C-ONO, \quad (21)$$

$$(C_xH_y)+O\rightarrow (C_{x-1}H_y)-C-O, \quad (22)$$

$$(C_xH_y)+OH\rightarrow (C_{x-1}H_y)-C-OH, \quad (23)$$

$$(C_{x-1}H_y)-C-NO_2\rightarrow (C_{x-1}H_y)+NO+CO, \quad (24)$$

$$(C_{x-1}H_y)-ONO\rightarrow (C_{x-1}H_y)+NO+CO, \quad (25)$$

$$(C_{x-1}H_y)-C-O\rightarrow (C_{x-1}H_y)+CO, \quad (26)$$

$$(C_{x-1}H_y)-C-OH\rightarrow (C_{x-1}H_{y-1})+CO+1/2H_2, \quad (27)$$

$$\beta HAP+(C_xH_y)\rightarrow \beta HAP-(C_xH_y), \quad (28)$$

$$\beta HAP-(C_xH_y)\rightarrow C_xH_y + \text{gas-phase decomposition products.} \quad (29)$$

The soot is assumed to contain only H and C atoms though actual soot may also contain O, N, and S. The reaction mechanism begins with the adsorption of NO_2 on soot forming C–NO_2 and C–ONO complexes. Adsorption of O and OH produces C–O and C–OH complexes. Spontaneous desorption produces CO (and a reduction of soot mass) and NO or H_2. The reaction of βHAPs with soot is what we call a deactivation process. The resulting desorption products are not further important to the process and so the reactivity of the βHAPs has been decreased. The kinetics of the adsorption reactions in Eqs. (20)–(23) and (28) is described in terms of reaction probability γ_i [$i=$(20–23), (28) for reactions (20)–(23), (28)]. These probabilities depend on the surface density of free adsorption sites $[s]$. We assumed a simple linear dependence of the form $\gamma_i=\gamma_{i-0}[s]/[s]_0$ where γ_{i-0} and $[s]_0$ are the reaction probability and the surface density of free adsorption sites at zero coverage of adsorbates. We chose $\gamma_{22-0}=0.12$ and $\gamma_{23-0}=0.1$ for O and OH based on Refs. 24 and 25. There is more uncertainty on the reaction probabilities for NO_2 (γ_{20-0} or γ_{21-0}). Experimental studies of different carbonaceous particles have produced γ_{21-0} of $5\times 10^{-3}-0.5$. We used $\gamma_{21-0}=0.1$ from the

experimental measurements of Smith and Chughtai for hexane soot as a base value.[20] The choice of this value was motivated by the fact that *n*-hexane soot is a good model for the soot found in diesel exhausts. However, since $\gamma_0(NO_2)$ may vary with the soot structure and the exhaust composition, we performed a parametric study of this parameter.

The rate constants of the desorption reactions in Eqs. (24) and (25) were deduced from the experiments of Tabor, Gutzviller, and Rossi.[26] Frequencies of 100–500 s^{-1} were determined for NO desorption following NO_2 adsorption on different carbonaceous particles at 300 K taking into account both the $(C_xH_y)-NO_2$ and $(C_xH_y)-ONO$ channels. These values represent a lower limit since the gas temperature in exhausts at the point of processing is around 453 K which should result in higher desorption frequencies. Consequently, a parametric study was performed on the NO desorption frequency. Since the rate limiting step of the oxidation of soot by either O atoms or OH radicals is the adsorption step, an arbitrary value of 10^8 s^{-1}, consistent with a fast desorption process, was used for the frequency of reactions in Eqs. (26), (27), and (29).

C. Electron/ion attachment to the soot

Soot particle charging by the attachment of charged species may affect the ionization kinetics, and therefore the electron temperature and density, in DBDs. Particle charging in plasmas has been mostly investigated at low pressure where the orbit motion limited (OML) theory may be used.[30] The validity of OML theory requires that $d_p \ll \lambda_D \ll \lambda_{mfp}$, where d_p is the particle diameter, λ_D is the Debye length of the plasma and λ_{mfp} is the electron/ion mean free path between collisions. For these conditions, the motion of charged species in the plasma sheath around the particle is collisionless and is mainly governed by the interaction potential between the particles and electrons or ions. In this case, the sheath potential and currents to the particles are functions only of the plasma density, electron temperature and ion temperature.

Unfortunately, the assumptions for the OML theory are violated by atmospheric plasmas. During the current pulse the electron density n_e and temperature T_e are $10^{12}-10^{13}$ cm^{-3} and 3–4 eV, which produces a Debye length of the order of 10^{-3} cm. The electron mean free path, based on N_2, is $\approx 3\times 10^{-5}$ cm and so the sheath is collisional.

To estimate an upper limit to the particle charging during the short current pulse, we considered the charging due to ion collection and electron attachment to the soot. The collection frequency of electrons by the soot is determined by assuming that the electron density in the sheath follows a Boltzmann distribution with respect to the electrical potential. The charging rate is then

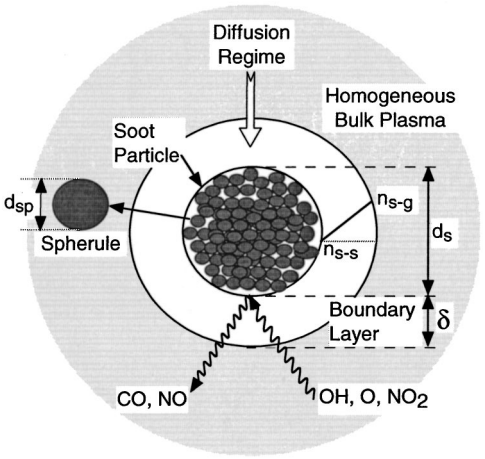

FIG. 2. Schematic of the quasihomogeneous gas-phase model used in GLOBAL_KIN to account for soot particles. The region surrounding the soot is divided into two zones—a homogeneous bulk gas-phase and a gas-surface boundary layer.

$$\frac{dQ_s}{dt} = -q\frac{n_{e-g}\exp(qV_s/kT_e)}{4}\sqrt{\frac{8kT_e}{\pi m_e}}\pi d_s^2 + \sum_i q_i \frac{n_{i-g}(1-\exp(q_iV_s/kT_i))}{4}\sqrt{\frac{8kT_i}{\pi m_i}}\pi d_s^2, \tag{30}$$

where d_s and Q_s denote the diameter and the electrical charge for the soot particles, q is the elementary charge and k is Boltzmann's constant. The terms m_e, n_{e-g}, and T_e are the electron mass, density in the bulk plasma and temperature, respectively, and m_i, n_{i-g}, q_i and T_i are the ion mass, density in the bulk plasma, charge and temperature, respectively. The sum is over ions. V_s is the particle potential and may be estimated from the particle charge by modeling the particle as a spherical capacitor

$$V_s = \frac{2qQ_s}{4\pi\epsilon_0 d_s}. \tag{31}$$

D. Reactions near and on particles

The exhaust in the DBD reactor is assumed to be perfectly stirred. The reactive medium around a given soot particle is described using a quasihomogeneous model which distinguishes two regions in the gas volume surrounding one particle: a homogeneous bulk gas phase and a gas-surface boundary layer (see Fig. 2). Using this assumption, the concentration profile in the boundary layer is linear between the gas phase and surface of the particles, and is mainly driven by diffusion and surface reactions. All the particles have the same diameter, d_s, that corresponds to the average of the actual particle diameter distribution. The soot particles are characterized by their diameter and by the surface density of available adsorption sites. The soot particle number density, n_p, is a constant since additional particle nucleation does not take place. The only physical change that particles undergo is a decrease of their diameter due to oxidation reactions.

Gas-phase species are characterized by their density in the bulk of the gas phase, n_{s-g}, and near the surface of the soot particles, n_{s-s}.

The time evolution of the bulk density of species i is given by

$$\frac{dn_{i-g}}{dt} = W_{i-g} + W_{i-s}, \tag{32}$$

where n_{i-g} and W_{i-g} are the bulk density and the net production rate by gas-phase reactions of species i. W_{i-s} denotes the net production term of species i by heterogeneous processes on the soot particles. This term is nonzero only for species involved in the surface reactions in Eqs. (20)–(29): O, OH, NO_2, NO, CO, H_2, and possibly βHAPs.

For large particle diameters, $d_s > 80$ nm, the continuum approach is valid and the source term W_{i-s} is directly related to the diffusion rate of species i at the soot surface

$$W_{i-s} = \left(-D_i \frac{n_{i-g} - n_{i-s}}{\delta} \right) \left(\pi d_s^2 n_p \right), \tag{33}$$

where D_i is the diffusion coefficient of species i and δ the boundary layer thickness. The first term of Eq. (33) is the rate of diffusion of species i to the soot particle. The second term is the soot geometric surface per unit volume of the gas phase. The diffusion boundary layer thickness may be estimated from a standard correlation for mass transfer between a fluid and an immersed sphere. For the conditions of interest

$$\mathrm{Nu} = 2.0 + 0.60 \mathrm{Re}^{1/2} \mathrm{Sc}^{1/3}, \tag{34}$$

where, $\mathrm{Nu} = d_s/\delta$ is the Nusselt number, $\mathrm{Re} = \rho \nu d_s/\mu$ is the Reynolds number, and $\mathrm{Sc} = \mu/\rho D_s$ is the Schmidt number.[31] The terms ρ, ν, and μ denote the mass density, velocity, and the viscosity of the gas phase. For the conditions considered in this work Re and Sc are small, and so the boundary layer thickness is nearly equal to the particle radius.

Since gas-phase chemistry is neglected in the boundary layer, the time variation of the density near the soot particle is governed by the balance between the flux of species entering the boundary layer by diffusion and the consumption or production of species by heterogeneous reactions at the soot surface. The mass balance in the boundary layer is

$$\frac{d}{dt}\left[\frac{1}{2} (n_{i-g} + n_{i-s}) V_\delta \right] = D_i \frac{n_{i-g} - n_{i-s}}{\delta} \pi d_s^2 + (R_{\mathrm{di}} - R_{\mathrm{ai}}) S_s, \tag{35}$$

where S_s is the specific surface of the soot particles and V_δ is the volume of the boundary layer. R_{di} and R_{ai} are the rates of desorption and adsorption per unit surface of soot for species i. The consumption rate by adsorption reactions is

$$R_{\mathrm{ai}} = \sum_j \left(a_{ij}^{(1)} \gamma_j v_i \frac{n_{i-s}}{4} \right), \tag{36}$$

where γ_j is the adsorption probability for the jth process and v_i the thermal speed of species i at the surface of the soot particle, $v_i = \sqrt{8kT_g/\pi m_i}$. The production rate of species i due to desorption reactions is

$$R_{\mathrm{di}} = \sum_j (a_{ij}^{(2)} k_j N_{i-s}), \tag{37}$$

where k_j is the rate of the jth desorption reaction and N_{i-s} is the surface density of the adsorbed species. The surface used in the computation of desorption and adsorption rates is the true surface area, S_s, of the soot, $S_s = \pi d_{\mathrm{sp}}^2 N_{\mathrm{sp}}$, where d_{sp} is the spherule diameter and N_{sp} is the number of spherules contained in each particle. This is consistent with the measurements of the adsorption probability and the surface density of the total adsorption sites.[20,26,27] The soot specific surface S_s was determined from experiments reporting that the particles are composed of $\approx$20 nm elementary spherules having a fractal structure.[17] A fractal dimension of $f = 2.8$ was chosen based on work by Mitchell and Frenklach.[32] The number of spherules, N_{sp}, contained in each particle is[33]

$$N_{\mathrm{sp}} = \left(\frac{d_s}{d_{\mathrm{sp}}} \right)^f. \tag{38}$$

The specific surface of the soot particles is assumed to be equal to the total surface of all the spherules. For estimating diffusion fluxes, the geometric surface was used.

The surface densities of the adsorbates are obtained from

$$\frac{dN_{i-s}}{dt} = \sum_j \left(a_{ij}^{(2)} \gamma_j v_i \frac{n_i'}{4} \right) - \sum_j (a_{ij}^{(1)} k_j N_{i-s}), \tag{39}$$

where the first sum is over adsorption reactions, the second sum is over the desorption reactions and n_i' is the density of the gas-phase species involved in the adsorption reaction.

A single type of adsorption site was used for all adsorbates. The total surface density of adsorption sites for OH and O has been reported to be $\approx 10^{15}$ cm^{-2} [34] which is similar to that for the adsorption sites of NO_2.[26] We therefore used 10^{15} cm^{-2} for the total surface density of the adsorption sites.

When the soot particle diameters are small and produce a Knudsen number, $\lambda_{\mathrm{mfp}}/d_s > 1$, the continuum approach is no longer valid. Diffusion is fast enough to insure a constant concentration in the boundary layer, $n_{i-s} = n_{i-g}$.[35] There is consequently no need for an equation for the densities of gas-phase species near the soot particles. The rate of surface reactions W_{i-s} is

$$W_{i-s} = (R_{\mathrm{di}} - R_{\mathrm{ai}}) S_s n_p, \tag{40}$$

where the factor $S_s n_p$ is the soot surface per unit volume.

The calculation of R_{ai} is different from that in the continuum regime since the rarefaction around the particle must be taken into account. In this case, R_{ai} is given by[35]

$$R_{\mathrm{ai}} = \sum_j \frac{2D_i}{8D_i/\gamma_j v_i + d_s/(1 + 2\Delta/d_s)} n_i, \tag{41}$$

where Δ is the mean distance between the point of last collision in the gas phase and the particle center.

At each step during the time integration in the model, the decrease of the soot mass is computed and the corresponding surface and diameter are adjusted assuming that the fractal dimension, and therefore the number of spherules, remain

constant. The soot number density also remains constant. When the size of the particle decreases to the point that the flow around the particles is not continuum [Eq. (36)]. Eqs. (40) and (41) are used to provide the heterogeneous rates.

III. NO_x PLASMA REMEDIATION IN THE PRESENCE OF SOOT

The gas is treated by a single discharge pulse having a duration $\approx 10^{-7}$ s consistent with DBDs. The time evolution of the exhaust is followed for a reactor gas residence time of 0.2 s. The initial composition of the exhaust gas is $N_2/O_2/H_2O/CO_2 = 79/8/6/7$ with 400 ppm of CO, 260 ppm of NO, 133 ppm of H_2, 500 ppm of propene and 175 ppm of propane. The base case values are an energy deposition of 38 J/L, soot particle density of 10^8 cm^{-3}, and soot particle diameters of 100 nm. The adsorption probability of NO_2 and the desorption rate constants are $\gamma_{21-0} = 0.1$ and $k_d = 500$ s^{-1}, respectively.

The fundamental processes initiating the plasma chemistry are the electron-impact dissociation of O_2, N_2, H_2O, and CO_2. The electron density n_e and temperature T_e are shown in Fig. 3(a) for the base case conditions. T_e rises to 3 eV until electron avalanche increases the conductivity of the plasma and T_e begins to decrease. The electron density n_e reaches 10^{13} cm^{-3} at which time the dielectric charges, thereby removing voltage from the gap. This reduces the electric field and T_e below the self-sustaining value. The electron density then quickly decays by attachment and recombination. The densities of O, OH, and N are shown in Fig. 3(b). Electron impact on O_2, N_2, and H_2O produces O, N, and OH, respectively [Eqs. (2)–(4)]. O is also produced by the electron impact dissociation of CO_2

$$e + CO_2 \rightarrow CO + O + e. \tag{42}$$

The peak O density is $\approx 10^{15}$ cm^{-3}. O is quickly consumed by O_2 to form ozone

$$O + O_2 + M \rightarrow O_3 + M. \tag{43}$$

N densities are smaller, $\approx 8 \times 10^{13}$ cm^{-3}, due to the higher threshold energy for the dissociation of N_2. N is dominantly consumed by the reaction with NO [Eq. (5)]. The peak OH density is $\approx 10^{14}$ cm^{-3}. OH is dominantly consumed by reactions with UHCs [Eqs. (8) and (9)]. Other nonhydrocarbon species that convert NO to NO_2 are HO_2 [Eq. (12)] and O_3

$$O_3 + NO \rightarrow NO_2 + O_2. \tag{44}$$

The time evolution of HO_2 and O_3 is shown in Fig. 3(c). HO_2 is sustained as an intermediate of the reactions of NO with the βHAPs [Eqs. (16) and (18)] and by the reaction of HCO with O_2

$$HCO + O_2 \rightarrow HO_2 + CO. \tag{45}$$

The densities of NO and NO_2 with and without heterogeneous reactions on the soot particles are shown in Fig. 4. The densities of OH and βHAP radicals are shown in Fig. 5. For $t < 10^{-6}$ s, the species that initiate the NO_x chemistry, HO_2, O_3, and the βHAP radicals, have a low density and NO and NO_2 densities remain nearly constant. For $t > 10^{-6}$ s, homogeneous reactions dominate and result in an almost total conversion of NO to NO_2 when heterogeneous processes are not taken into account. When surface reactions are included, the densities of NO and NO_2 critically depend on the probability of reaction with βHAP radicals. In the absence of βHAP deactivation, heterogeneous reactions slow down the total rate of NO→NO_2 conversion by the generation of NO on the particles. For example, the exit NO density is ≈50 ppm compared to ≈5 ppm when soot particles are not considered. The heterogeneously generated NO comes from the adsorption of NO_2 on the particles, followed by reduction of NO_2 and desorption. This is accompanied by a 35% decrease in NO_2 concentration.

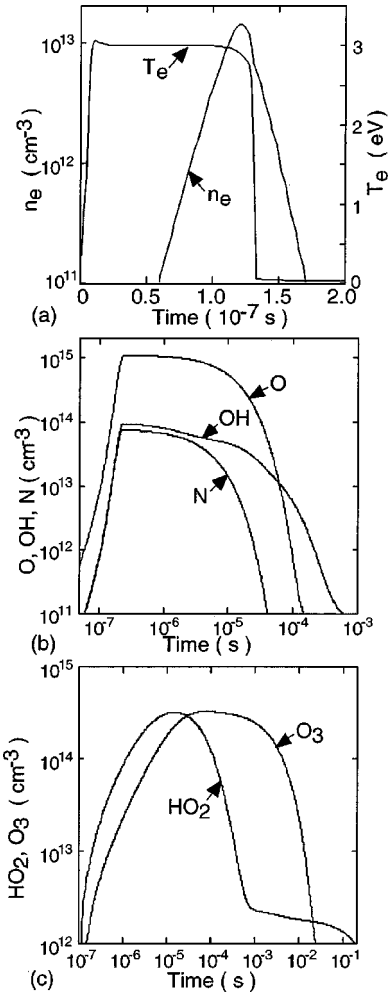

FIG. 3. Time evolution of plasma parameters and plasma chemistry initiating species. (a) The electron density, n_e, and temperature, T_e. (b) N, OH, and O. (c) HO_2 and O_3. Figures correspond to the base case conditions—energy deposition of 38 J/L, initial gas mixture of $N_2/O_2/H_2O/CO_2 = 79/6/8/7$ with 400 ppm CO, 133 ppm H_2 and 260 ppm NO (1 atm, 453 K), soot particle number density of 10^8 cm^{-3} and diameter of 100 nm.

When the adsorption of βHAPs is included with $\gamma_{28-0} = 1.0$, the effect of soot is more pronounced. The NO→NO_2 homogeneous conversion produces a minimum in the density of NO of 1.9×10^{15} cm^{-3} at $t \approx 10^{-2}$ s and then increases to 3.3×10^{15} cm^{-3}, keeping NO as the major NO_x species. As a result of βHAP deactivation on soot, βHAP densities decrease to 2.8×10^{14} cm^{-3} by 10^{-2} s (see Fig. 5). This decreases the rate of oxidation of NO by βHAP [Eqs. (13) and

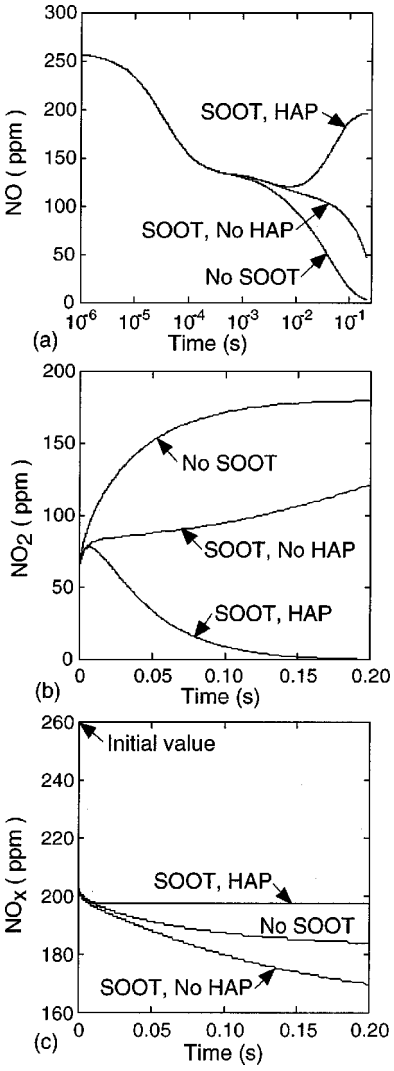

FIG. 4. Time evolution of NO_x species without soot (No SOOT), with soot (SOOT, No HAP) and with soot+βHAP deactivation on soot (SOOT, HAP). (a) NO. (b) NO_2. (c) NO_x. The presence of soot improves NO_x remediation through the increased production of HNO_2. With βHAP deactivation on soot, the exit concentration of NO_x is higher compared to the no-soot case because of the decreased production of OH. Conditions are the same as for Fig. 3.

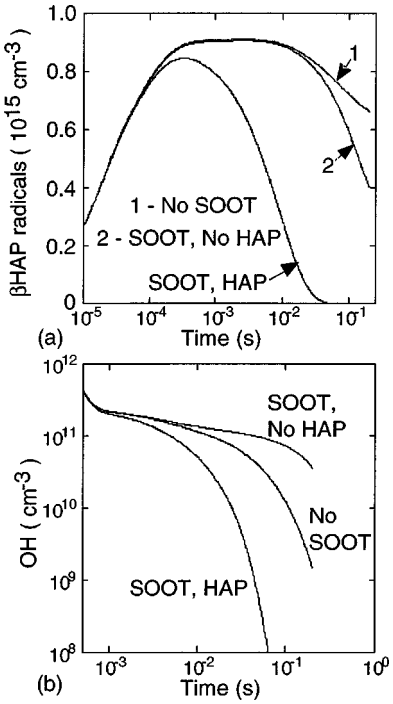

FIG. 5. Time evolution of radicals involved in NO remediation. (a) βHAPs and (b) OH for the cases without soot, with soot and with soot+βHAP deactivation. In the presence of soot and without βHAP deactivation, OH densities are higher and as a result aid in NO_x remediation through the formation of HNO_2. With βHAP deactivation, the rate of reactions in the NO_x-soot reaction cycle is decreased leading to a decreased production of OH. Conditions are the same as for Fig. 3.

(14)] which in turn decreases the rate of production of NO_2. The end result is a rebound in the density of NO.

The change in total NO_x concentration is shown in Fig. 4(c). The unresolved drop in NO_x of $\approx$15 ppm when including soot chemistry without βHAP deactivation is due to the increased conversion of NO to HNO_2. This is facilitated by an increase of OH density when soot is included, as shown in Fig. 5(b). When both NO_2-soot reactions and βHAP radical deactivation are taken into account, NO_x removal decreases by $\approx$10%. This change is mainly due to the decrease of OH radical concentration, as shown in Fig. 5(b). This decrease in OH is due to the decrease in the production of OH from βHAPs [pathways (13)-(15)-(16)-(12) and (14)-(17)-(18)-(12)]. Since βHAP deactivation decreases the gas-phase concentration of βHAP, the rates of the subsequent reactions in the pathways are also decreased. The rate of NO$\rightarrow$HONO conversion [Eq. (19)] is proportional to the density of OH which is dominantly produced from HO_2 through the reaction in Eq. (12). The main sources of HO_2 are the reactions between βHAP radicals and NO through the reaction pathways (13)-(15)-(16) and (14)-(17)-(18). Therefore the deactivation of βHAPs leads to the decrease in HO_2 and OH densities, which in turn slows the rate of homogeneous oxidation of NO and NO_2.

The reaction of soot with NO_2 also affects the C_3H_6, HCHO and CH_3CHO densities as shown in Fig. 6. When $\gamma_{28-0}=0$ for βHAPs, the C_3H_6 density decreases by $\approx$25% compared to the no soot case. This is due to the increase of the OH concentration [see Fig. 5(b)] which produces an increase in the consumption of C_3H_6 through the reactions in Eqs. (8) and (9). Simultaneously, the densities of formaldehyde and acetaldehyde increase by factors of 2 and 3. This is due to the higher NO density which leads to an increase in production of HCHO and CH_3CHO through the reaction pathways (13)-(15)-(16) and (14)-(17)-(18). When $\gamma_{28-0}=1$ for βHAPs, the decrease of the OH density lowers the reaction rate between OH and C_3H_6. Consequently, the C_3H_6 density is 12% higher than the case without soot. Smaller densities for HCHO and CH_3CHO are also generated due to the lower rate of reaction of OH with C_3H_6, the initiating reaction for the production of these species.

The heterogeneous interaction of NO_2, O, and OH with soot particles leads to the formation of CO. The densities of CO with and without soot particles are shown in Fig. 7(a). The heterogeneous production of CO starts at $t\approx10^{-4}$ s when desorption of NO from the particles becomes impor-

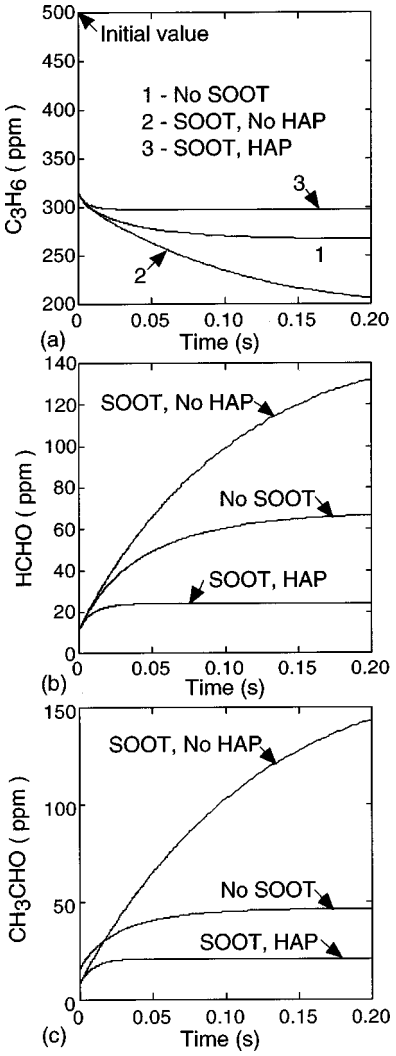

FIG. 6. Time evolution of UHCs and end products of the remediation process. (a) C_3H_6, (b) HCHO, and (c) CH_3CHO for the cases without soot, with soot, and with soot+βHAP deactivation. In the presence of soot and no βHAP deactivation, C_3H_6 concentrations are smaller due to the increased consumption by reactions with OH. This in turn, leads to increased production of HCHO and CH_3CHO, the final products of NO-βHAP reaction. With βHAP deactivation, OH production decreases leading to lesser C_3H_6 consumption and a lower production of HCHO and CH_3CHO. Conditions are the same as for Fig. 3.

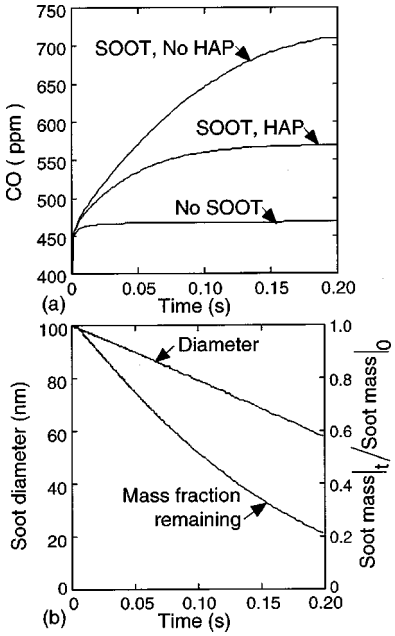

FIG. 7. Time variation of soot oxidation products and soot properties. (a) CO production for the cases without soot, with soot, and with soot+βHAP deactivation. (b) Soot diameter and fractional reduction in soot mass. Conditions are the same as for Fig. 3. In the presence of soot, more CO is produced due to the oxidation of soot by NO_2. With βHAP deactivation, less NO_2 is produced due to the heterogeneous loss of βHAP on soot. As a result, less CO is produced compared to the soot-no βHAP case. However, compared to the no-soot case, CO production is increased due to the additional heterogeneous CO source by NO_2 adsorption.

tant. Consequently, without βHAP deactivation, the exit CO concentration is ≈65% larger than the case without soot. The production of CO is assisted by the dynamics of NO↔NO_2 exchange involving homogeneous NO→NO_2 conversion in the gas phase and heterogeneous NO_2→NO conversion on soot. For each cycle of this exchange ($NO_{2(gas)}$→$NO_{2(soot)}$ →$NO_{(gas)}$), one CO molecule is generated. When $\gamma_{28-0}=1$ for βHAP, the increase of CO concentration is ≈20% since the NO↔NO_2 exchange rate is slower due to the decrease of βHAP and HO_2 densities.

The desorption of CO produces a loss of soot mass shown in Fig. 7(b). The mass of soot is decreased by a factor of 3.5 with a diameter reduction of ≈45%. The mass loss is initiated by reactions with NO_2 which account for ≈99.9% of the loss. Less soot is consumed when $\gamma_{28-0}=1$ for βHAP. In this case, the βHAPs are mainly consumed through deactivation on soot particles, which leads to a decrease of the NO→NO_2 conversion rate and slower NO↔NO_2 exchange dynamics.

The densities of adsorbed species are shown in Fig. 8 for the case with no βHAP deactivation. The adsorption sites are not saturated. The surface densities of NO_2 adsorbates reach a quasi-steady state value of $\approx 6\times 10^{14}$ cm^{-2} at $t\approx 10^{-3}$ s at which time the limiting step for the NO_2→NO heterogeneous conversion is the desorption of NO. The surface densities of O and OH are smaller compared to NO_2 due to the higher homogeneous loss frequencies of O and OH and the spontaneous desorption of $O_{(ads)}$ and $OH_{(ads)}$.

In the simulations discussed thus far, electron and ion attachment to soot were not considered. The n_e and T_e are

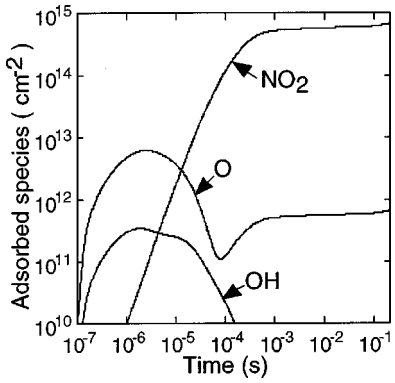

FIG. 8. Time evolution of the adsorbed species, O, OH, and NO_2. Conditions are the same as for Fig. 3.

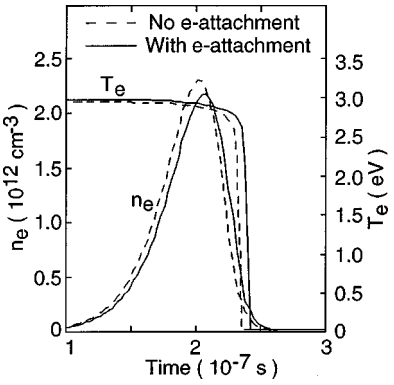

FIG. 9. Electron attachment to soot. The n_e and T_e for a soot particle density of 10^9 cm^{-3} and an initial particle diameter of 150 nm. Other conditions are the same as for Fig. 3. The electron temperature increases slightly in the presence of soot to increase ionization rates to account for losses to the soot.

shown for particle density of 10^9 cm^{-3} and soot diameter of 150 nm in Fig. 9 with and without particle charging. At this higher surface density of soot, there is $\approx$5% decrease in n_e and a small increase in T_e to increase the ionization rate to offset the electron loss to the particles. The effect is proportionally smaller for the smaller soot surface density of the base case. The consequence of these changes on the active species in NO_x chemistry is small and does not appreciably affect the results reported in this section.

The soot affects NO_x chemistry through the kinetics of NO_2 absorption and NO desorption. Since the adsorption probability and the soot surface may change during the treatment of the exhaust, it is instructive to parametrize the initial NO_2 adsorption probabilities [γ_{20-0} and γ_{21-0} collectively called $\gamma_0(NO_2)$], the NO desorption frequency [k_d(C–ONO) and k_d(C–NO_2) collectively called k_d(NO)] and the initial active soot surface per unit gas-phase volume (the product of the soot active surface and the soot particle density, $S_s n_p$).

The exit densities of NO and NO_2 as a function of $\gamma_0(NO_2)$ for different values of k_d(NO), with $\gamma_{22-0}=0$ for βHAPs, are shown in Fig. 10. For low k_d, NO increases monotonically with $\gamma_0(NO_2)$. Larger rates of NO_2 adsorption produce more NO generation. Most of the NO is converted to NO_2 in the gas phase thereby showing a monotonic decrease with $\gamma_0(NO_2)$. For $k_d(NO) \geqslant 1000$ s^{-1}, the density of NO first increases with $\gamma_0(NO_2)$, reaches a maximum and then decreases at high $\gamma_0(NO_2)$ values. In the low $\gamma_0(NO_2)$ range the soot particles' diameter does not change significantly and the main consequence of increasing the adsorption probability is the production of more NO. Above a critical adsorption probability, the NO_2-soot reaction results in a decrease of soot particle diameter as shown in Fig. 11(a). This reduction in the specific surface area reduces the rate of NO$\rightarrow$NO heterogeneous conversion. Consequently, the homogeneous NO$\rightarrow NO_2$ conversion dominates over the heterogeneous $NO_2\rightarrow$NO conversion, which leads to a smaller density for NO. The final NO concentration as a function of $\gamma_0(NO_2)$ is not affected by the desorption frequency when $k_d > 10^4$ s^{-1}. This indicates that the limiting step in $NO_2 \rightarrow$NO heterogeneous conversion is the adsorption step. The

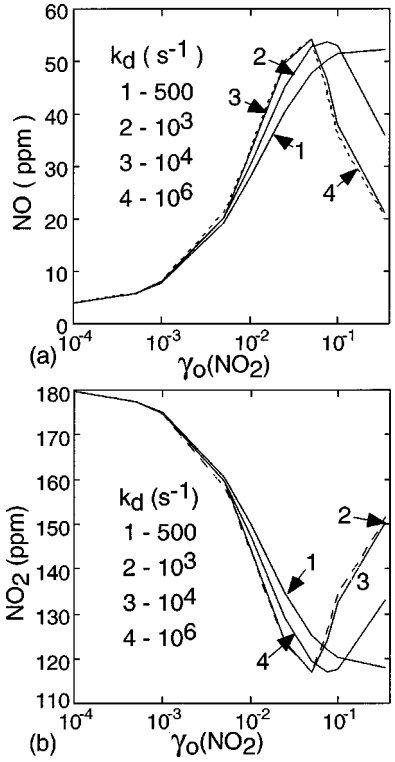

FIG. 10. Exit concentrations as a function of $\gamma_0(NO_2)$ for different values of $k_d(NO_2)$. (a) NO. (b) NO_2. Conditions are the same as for Fig. 3 with no βHAP deactivation.

decrease in soot diameter with increasing $\gamma_0(NO_2)$ is a result of the more rapid rate of heterogeneous reactions which bind with C in the soot, ultimately leading to the production of CO. As k_d(NO) increases, the fraction of unoccupied surface

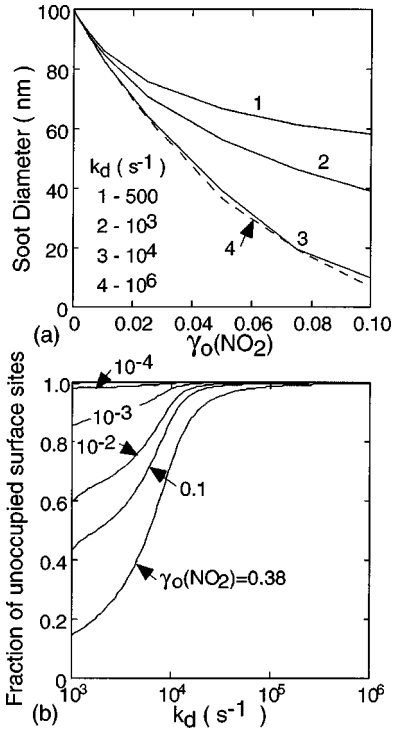

FIG. 11. Change in soot properties as a function of $\gamma_0(NO_2)$ and $k_d(NO_2)$. (a) Soot diameter. (b) Fraction of unoccupied surface sites.

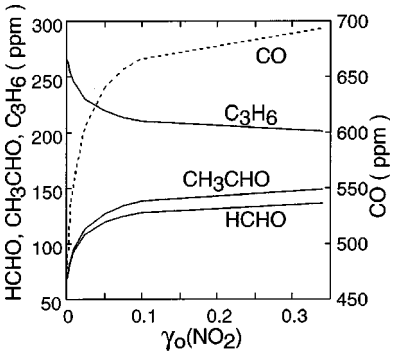

FIG. 12. Exit densities of HCHO, CH_3CHO, C_3H_6, and CO as a function of $\gamma_0(NO_2)$. With increasing adsorption probabilities of NO_2, the production of HCHO, CH_3CHO, and CO increase and the consumption of C_3H_6 also increases due to the indirect increase in OH production.

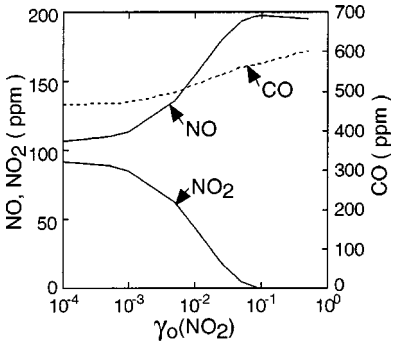

FIG. 13. Variation of NO, NO_2, and CO with $\gamma_0(NO_2)$ for full βHAP deviation. As $\gamma_0(NO_2)$ increases, more NO_2 is adsorbed leading to an increased gas-phase concentration of NO. This also leads to an increased oxidation of soot resulting in increased CO production. Other conditions are the same as for Fig. 3.

sites increases, as shown in Fig. 11(b), thereby enabling more rapid adsorption of NO_2. When $k_d(NO) > 10^4\ s^{-1}$, the adsorption of NO_2 becomes the rate-limiting step in the oxidation of soot. This results in low surface densities of NO_2 and so the oxidation of soot saturates.

The variation of the total NO_x density with $\gamma_0(NO_2)$ closely follows that of NO_2. In particular, a 15% increase in NO_x remediation is obtained when $\gamma_0(NO_2)$ increases from 10^{-4} to 0.1. The increase in $\gamma_0(NO_2)$ also produces significant changes in CO, C_3H_6, HCHO and CH_3CHO densities, as shown in Fig. 12. These densities are almost independent on the NO_2 desorption frequency and values are shown for $k_d(NO_2) = 10^3\ s^{-1}$. The increase of $\gamma_0(NO_2)$ in the range 10^{-4}–0.1 leads to a 50% increase of CO and more than a 100% increase for HCHO and CH_3CHO. The concentration of C_3H_6 decreases by almost 25%. The increase of CO is a direct consequence of the increase of adsorption of NO_2 leading to NO and CO desorption. The increase in HCHO and CH_3CHO when increasing $\gamma_0(NO_2)$ is a consequence of the enhancement of NO-βHAP reactions in Eqs. (13) and (14) resulting from the increase in NO. These reactions also ultimately increase the OH density which increases the rate of reactions between OH and C_3H_6 [Eqs. (8) and (9)], which then decreases the C_3H_6 density.

When $\gamma_{22-0} = 1$ for βHAP, the densities of NO and NO_2 as a function of $\gamma_0(NO_2)$ have a weak dependence on k_d. The NO concentration increases by almost 90% when $\gamma_0(NO_2)$ is varied from 10^{-4} to 0.1, as shown in Fig. 13, while the NO_2 concentration decreases. When βHAP radicals are totally quenched by the soot, the NO_x chemistry is similar to that in the absence of UHCs. This results in a slower rate of $NO \rightarrow NO_2$ homogeneous conversion, which also leads to a slower $NO_2 \leftrightarrow NO$ exchange dynamics. As a result, the effect of the NO released from the soot is less pronounced on the densities of the other species (e.g., C_3H_6) as compared to the $\gamma_{22-0} = 0$ case. The densities of HCHO and CH_3CHO, which are produced by NO-βHAP reactions, are almost one order of magnitude smaller than in the case for $\gamma_{22-0} = 0$ for βHAP. The production of CO is commensurately smaller.

The surface of soot particles per unit volume is one of the key parameters in the model. The average diameter of soot particles in diesel exhaust is usually 90–120 nm while the particle density can vary by orders of magnitude depending on the combustion regime or the type of engine.[17–19] The variation of the exit NO and NO_2 concentration as a function of particle density is shown in Fig. 14(a) for $\gamma_0(NO_2) = 0.1$. The increase of n_p leads to an increase of NO and a decrease of NO_2 due to the larger surface area available for NO_2 adsorption. The heterogeneous reaction chemistry becomes significant for $n_p > 5 \times 10^7\ cm^{-3}$. NO becomes the major exit NO_x species when $n_p > 2 \times 10^8\ cm^{-3}$. The NO density saturates for $n_p > 10^9\ cm^{-3}$ due to depletion of NO_2.

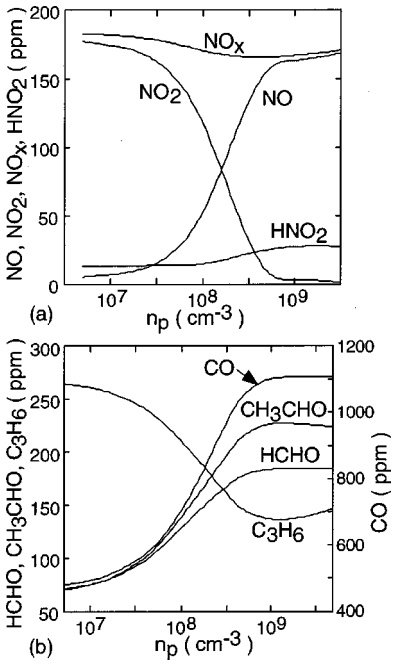

FIG. 14. Effect of soot particle number density on $NO_x/C_xH_yO_z$. (a) NO, NO_2, NO_x, and HNO_2. Increased soot number density increases the rate of heterogeneous $NO_2 \rightarrow NO$ conversion resulting in higher NO concentrations. NO_x densities decrease with n_p due to the increased production of HNO_2. (b) HCHO, CH_3CHO, C_3H_6, and CO. Increasing n_p increases the surface area for heterogeneous reactions resulting in increased production of OH which increases the rate of reaction with C_3H_6. As a result more of HCHO and CH_3CHO are produced. CO increases due to the increased rate of soot oxidation.

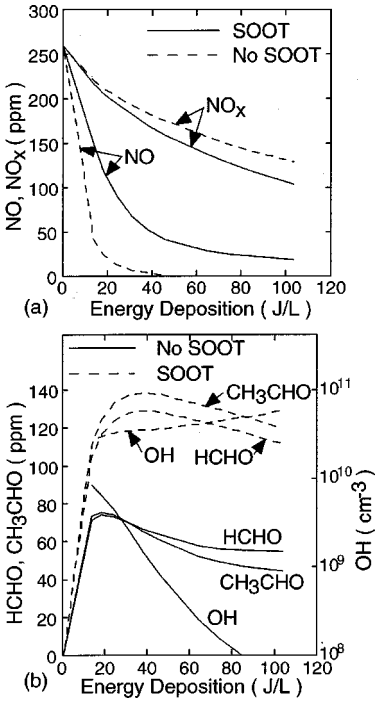

FIG. 15. Effect of energy deposition on $NO_x/C_xH_yO_z$. (a) Exit concentrations of NO, NO_x with and without soot. NO_x remediation improves in the presence of soot due to the increased production of HNO_2. In the presence of soot NO is not completely remediated due to the heterogenous back conversion of NO_2 to NO. (b) Exit concentrations of HCHO, CH_3CHO, and OH with and without soot. With increasing energy deposition, more OH is produced due to the increased rates of the dissociation of H_2O. However, in the presence of soot, higher OH densities are sustained due to the increased production of HO_2.

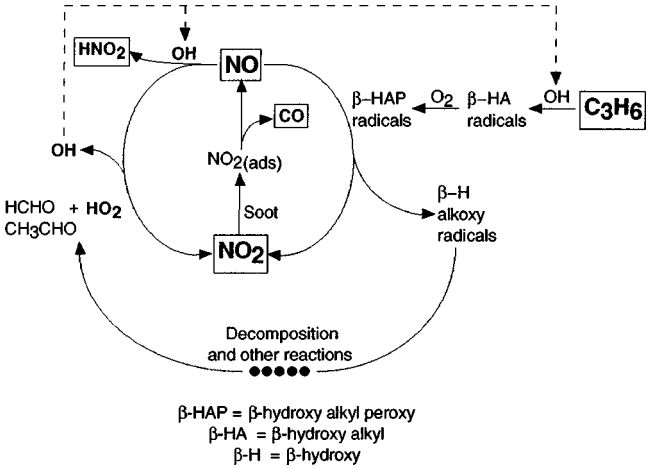

FIG. 16. Summary of the effects of soot on homogeneous NO_x chemistry. Heterogenous reactions on soot surfaces result in higher NO densities in the gas phase which increases the rates of the reaction with βHAPs. This leads to increased production of aldehydes and HO_2. HO_2 further reacts with NO by $HO_2+NO\rightarrow NO_2+OH$ to increase the production of OH. This increases the production of HNO_2 and the conversion of C_3H_6 thereby improving NO_x remediation and UHC consumption.

Except for $n_p>5\times10^9$ cm^{-3}, the increase of NO leads to a small increase in the remediation of NO_x and an increase of HNO_2. The higher production of HNO_2 is due to the increase of the densities of HO_2 and OH whose production is assisted by the $NO_2\leftrightarrow$NO exchange dynamics. The increase of NO results in higher rates of reactions with βHAPs [Eqs. (13) and (14)]. This ultimately results in the increase in the densities of HO_2, HCHO, and CH_3CHO through the reaction pathways (13)-(15)-(16) and (14)-(17)-(18) as shown in Fig. 14(b). The increase of NO and HO_2 leads to an increase in OH production [Eq. (12)] which results in more propene consumption [Eqs. (8) and (9)]. The increase in total particle surface area increases the concentration of carbon monoxide by a factor of 2.2 for $n_p=10^7-10^9$ cm^{-3}.

The results just discussed had $\gamma_{22-0}=0$ for βHAP. When $\gamma_{22-0}=1$ for βHAP, the results obtained are similar to those for $\gamma_0(NO_2)$ variation. In particular, the dynamics of the $NO_2\leftrightarrow$NO exchange slow down and there is no indirect effect of soot on the production of HO_2 and OH as observed for the $\gamma_{22-0}=0$ case.

The consequences of energy deposition by the plasma on the NO_x chemistry with and without soot are shown in Fig. 15. The peak O and OH densities increase linearly with increasing energy deposition. The increase in the production of these radicals increases the remediation of NO and NO_x. The decrease of NO with energy deposition is larger without soot particles due to the heterogeneous generation of NO with soot. Soot, however, generally improves NO_x remediation. This is due to the conversion of NO to HNO_2 through the reaction with OH [Eq. (19)]. As energy deposition increases, the exit HCHO and CH_3CHO densities decrease, both with and without soot, as shown in Fig. 15(b). This is due to the fact that with increasing energy more OH is generated which consumes more NO to form HNO_2. Thus the amount of NO reacting with βHAPs decreases and, consequently, HCHO and CH_3CHO, which are formed from the products of the reaction of βHAP with NO, also decrease.

The energy required for converting a given amount of NO to NO_2 before performing a catalytic reduction strongly depends on the soot particle density and is shifted to higher values when n_p is increased. Plasma treatment cannot generally reduce the NO concentration below a lower limit of $\approx$20–40 ppm if a large amount of soot is present in exhausts.

IV. CONCLUDING REMARKS

Results from a computational investigation of NO_x plasma remediation were used to discuss the consequences of heterogeneous chemistry on soot particles. For particle densities typical of diesel exhausts, $n_p=10^7-10^9$ cm^{-3}, the heterogeneous chemistry maintains the dynamic NO density which ultimately enables a higher NO_x remediation rate. The heterogeneous reactions also increase the production of carbon monoxide, formaldehyde and acetaldehyde. When the particle density is greater than 10^8 cm^{-3}, there may also be additional remediation of UHCs such as propene.

The effects of soot on the NO_x reaction mechanism are summarized in Fig. 16. Soot influences the NO_x chemistry by changing the NO/NO_2 ratio in the plasma. By regenerating the NO from NO_2 and by indirectly leading to the increase of OH radicals [Eq. (12)], soot increases the formation of HNO_2. This leads to an increased NO_x remediation. The increase in OH density also increases UHC consumption [Eqs. (8) and (9)]. The effect of soot strongly depends on the

disposition of βHAP radicals on particles. If βHAP adsorb on the particles with high probability, the homogenous chemistry is similar to that taking place without UHCs since these important intermediate radicals are consumed by the soot (or deactivated). The soot particles affect the NO_x chemistry mainly through the $NO_2 \rightarrow NO$ heterogeneous conversion. The effect of soot is much more complex in the case when the reactivity of βHAP radicals on the particles is small. In such a case, the combined effect of the heterogeneous NO_2 reactions and the homogeneous reactions in Eqs. (13) and (14) are reflected in the production of HNO_2 [Eq. (19)], formaldehyde [pathways (13)-(15)-(16) and (14)-(17)] and acetaldehyde [pathways (13)-(15) and (14)-(17)-(18)]. These dynamics also result in the remediation of UHCs and to the increase of CO in the exhaust.

The CO production is accompanied by a decrease in soot mass which, for most of the conditions discussed here, does not lead to a complete removal of soot particles. The soot particles also do not contain a significant amount of adsorbed NO_x for the desorption frequencies used in this work. Consequently, posttreatment of these particles would not lead to regeneration of NO_x. The presence of soot increases the amount of energy required for a given $NO \rightarrow NO_2$ conversion. For exhausts with high densities of soot particles, the variation of NO conversion with energy density shows a higher asymptotic value compared to the no soot case.

This work has clarified weakness in the database which should be addressed to more accurately investigate soot dynamics. In particular, a better description of the soot structure is necessary to more accurately model the surface reaction kinetics. The effect of the heterogeneous chemistry of water adsorption on soot particles should also be investigated, and the possible interactions between different adsorbates should be taken into account. The disposition of βHAP radicals on soot is a major issue which requires further investigation.

ACKNOWLEDGMENTS

This work was performed under the auspices of the UIUC-CNRS Collaboration Project ''Development of Novel Techniques to Remove and Recover Hazardous Air Pollutants from Gas Streams'' which supported K. H. The participation by R. D. and M. J. K. was supported by the Ford Motor Company and the National Science Foundation (CTS99-74962).

[1] B. M. Penetrante, R. M. Brusasco, B. T. Merritt, W. J. Pitz, G. E. Vogtlin, M. C. Kung, H. H. Kung, C. Z. Wan, and K. E. Voss, Society of Automotive Engineers, Paper 982508 (1998).
[2] J. W. Hoard and M. L. Balmer, Society of Automotive Engineers, Paper 982429 (1998).
[3] M. L. Balmer, R. Tonkyn, A. Kim, S. Yoon, D. Jimenez, T. M. Orlando, and S. E. Barlow, Society of Automotive Engineers, Paper 982511 (1998).
[4] J. W. Hoard, T. J. Wallington, J. C. Ball, M. D. Hurley, K. Wodzisz, and M. L. Balmer, Environ. Sci. Technol. **33**, 3427 (1999).
[5] M. B. Chang, M. J. Kushner, and M. J. Rood, Environ. Sci. Technol. **26**, 777 (1992).
[6] B. M. Penetrante, M. C. Hsiao, B. T. Merritt, G. E. Vogtlin, P. H. Wallman, M. Neiger, O. Wolf, T. Hammer, and S. Broer, Appl. Phys. Lett. **68**, 3719 (1996).
[7] H. Hamada, Y. Kintaichi, M. Sasaki, T. Ito, and M. Tabata, Appl. Catal. **70**, L15 (1991).
[8] J. O. Petunchi and W. K. Hall, Appl. Catal., B **2**, L17 (1993).
[9] T. Hammer, T. Kishim, H. Miessner, and R. Rudolf, Society of Automotive Engineers, Paper 993632 (1999).
[10] A. C. Gentile and M. J. Kushner, J. Appl. Phys. **79**, 3877 (1996).
[11] H. Russ, M. Nieger, and J. Lang, Trans. Plasma Sci. **27**, 38 (1999).
[12] B. M. Penetrante, M. C. Hsiao, B. T. Meritt, G. E. Vogtlin, and P. H. Wallman, Trans. Plasma Sci. **23**, 679 (1995).
[13] Y. S. Mok, S. W. Ham, and I. S. Nam, Trans. Plasma Sci. **26**, 1566 (1998).
[14] A. C. Gentile and M. J. Kushner, J. Appl. Phys. **78**, 2074 (1995).
[15] W. Niessen, O. Wolf, R. Schruft, and M. Neiger, J. Phys. D **31**, 542 (1998).
[16] R. Dorai and M. J. Kushner (to be published in J. Appl. Phys.).
[17] J. P. A. Neeft, M. Makkee, and J. A. Moulijn, Fuel Process. Technol. **47**, 1 (1996).
[18] V. T. Kerminen, T. E. Makela, C. H. Ojanen, R. E. Hillamo, J. K. Vilhunen, L. Rantanen, N. Havers, A. Von Bohlen, and D. Klockow, Environ. Sci. Technol. **31**, 1883 (1997).
[19] D. Kayes and S. Hochgreb, Environ. Sci. Technol. **33**, 3968 (1999).
[20] M. S. Akhter, A. R. Chughtai, and D. M. Smith, J. Phys. Chem. **88**, 5334 (1984).
[21] A. R. Chughtai, W. F. Welch, and D. M. Smith, Carbon **28**, 411 (1990).
[22] R. Dorai, M.S. thesis, University of Illinois, 2000, ⟨http://uigelz.ece.uiuc.edu/theses.html⟩.
[23] J. P. A. Neeft, T. Xander Nijhuis, E. Smakman, M. Makkee, and J. A. Moulijn, Fuel **76**, 1129 (1997).
[24] A. Harano, M. Sadakata, and M. Sato, J. Chem. Eng. Jpn. **24**, 100 (1991).
[25] T. Ngo, E. J. Sander, W. M. Tong, R. S. Williams, and M. S. Anderson, Surf. Sci. **314**, L817 (1994).
[26] K. D. Tabor, L. Gutzviller, and M. J. Rossi, J. Phys. Chem. **98**, 6172 (1994).
[27] M. Kalberer, K. Tabor, M. Ammann, Y. Parrat, E. Weingartner, D. Piguet, E. Rössler, D. T. Jost, A. Türler, H. W. Gäggeler, and U. Baltensperger, J. Phys. Chem. **100**, 15487 (1996).
[28] B. Aumont, S. Madronich, M. Ammann, M. Kalberer, U. Baltensperger, D. Hauglustaine, and F. Brocheton, J. Geophys. Res. **104**, 1729 (1999).
[29] D. M. Smith and A. R. Chughtai, Colloids Surf., A **105**, 47 (1995).
[30] J. Goree, Plasma Sources Sci. Technol. **3**, 400 (1994).
[31] R. B. Bird, W. E. Stewart, and E. N. Lightfoot, *Transport Phenomena* (Wiley, New York, 1960), Chap. 13.
[32] P. Mitchell and M. Frenklach, *Proceedings of the 27th International Symposium on Combustion* (The Combustion Institute, Pittsburgh, PA, 1998), pp. 1507–1514.
[33] J. Magill, J. Aerosol Sci. **22**, Suppl. 1 S165 (1991).
[34] P. Markatou, H. Wang, and M. Frenklach, Combust. Flame **93**, 467 (1993).
[35] J. Porstendörfer, G. Röbig, and A. Ahmed, J. Aerosol Sci. **10**, 21 (1978).